Type 2 alveolar cells are stem cells in adult lung

Christina E. Barkauskas,[1] Michael J. Cronce,[2] Craig R. Rackley,[1] Emily J. Bowie,[2] Douglas R. Keene,[3] Barry R. Stripp,[1] Scott H. Randell,[4] Paul W. Noble,[1] and Brigid L.M. Hogan[2]

[1]Division of Pulmonary, Allergy, and Critical Care Medicine, Department of Medicine, Duke University Medical Center, Durham, North Carolina, USA. [2]Department of Cell Biology, Duke University, Durham, North Carolina, USA. [3]Shriners Research Center, Portland, Oregon, USA. [4]Department of Cell Biology and Physiology, University of North Carolina at Chapel Hill School of Medicine, Chapel Hill, North Carolina, USA.

Gas exchange in the lung occurs within alveoli, air-filled sacs composed of type 2 and type 1 epithelial cells (AEC2s and AEC1s), capillaries, and various resident mesenchymal cells. Here, we use a combination of in vivo clonal lineage analysis, different injury/repair systems, and in vitro culture of purified cell populations to obtain new information about the contribution of AEC2s to alveolar maintenance and repair. Genetic lineage-tracing experiments showed that surfactant protein C–positive (SFTPC-positive) AEC2s self renew and differentiate over about a year, consistent with the population containing long-term alveolar stem cells. Moreover, if many AEC2s were specifically ablated, high-resolution imaging of intact lungs showed that individual survivors undergo rapid clonal expansion and daughter cell dispersal. Individual lineage-labeled AEC2s placed into 3D culture gave rise to self-renewing "alveolospheres," which contained both AEC2s and cells expressing multiple AEC1 markers, including HOPX, a new marker for AEC1s. Growth and differentiation of the alveolospheres occurred most readily when cocultured with primary PDGFRα$^+$ lung stromal cells. This population included lipofibroblasts that normally reside close to AEC2s and may therefore contribute to a stem cell niche in the murine lung. Results suggest that a similar dynamic exists between AEC2s and mesenchymal cells in the human lung.

Introduction

The lung is a complex organ with a large and highly vascularized epithelial surface area. Efficient gas exchange and host defense rely on the integrity of this epithelium and its dynamic interaction with surrounding mesenchyme. Lung cell turnover is normally slow compared with other adult organs such as the skin and intestine. However, significant regeneration and repair are possible after physiologic insults, including pneumonectomy and severe respiratory infection (1–4). Understanding the regenerative capacity of the lung and the role of resident stem and progenitor cells is therefore of considerable practical and therapeutic interest.

Here, we focus on the maintenance and repair of the distal gas exchange region of the lung that is composed of millions of alveoli organized into hundreds of clusters or acini (5). Each alveolus contains cuboidal type 2 epithelial cells (AEC2s) expressing high levels of surfactant protein C (SFTPC) and very thin type 1 cells (AEC1s) in close apposition to capillaries. Several pathologic conditions disrupt the delicate architecture of the alveoli — with loss of numbers in chronic obstructive pulmonary disease (COPD) (6) and their obliteration in idiopathic pulmonary fibrosis (IPF) (7). Data suggest that these pathologies are triggered in part by defects in the alveolar epithelium; increased apoptosis and senescence have been described in COPD (8, 9), and mutations associated with abnormal surfactant protein processing and ER stress have been reported in IPF and hereditary fibrotic lung disease (reviewed in ref. 10). These defects are thought to promote disease by reducing the normal reparative capacity of the alveolar epithelium, but precise information about underlying mechanisms is still lacking.

Historical data from simian and rodent models suggested that SFTPC$^+$ AEC2s function as progenitor cells in the alveoli and proliferate and differentiate into AEC1s (11, 12). Our recent genetic lineage-tracing studies in the mouse clearly established that SFTPC$^+$ AEC2s, as a population, proliferate in vivo and give rise to AEC1s (13). These data also showed that these processes, which are normally quite slow, are stimulated after injury with bleomycin, a chemotherapeutic agent that damages multiple cell types in the alveoli and induces transient inflammation and fibrosis (14).

In spite of this progress, many important questions remain regarding the identity, behavior, and regulation of alveolar epithelial progenitors. For example, do SFTPC$^+$ AEC2s have the capacity to undergo self renewal and differentiation over many months, thereby meeting the definition of long-term tissue stem cells? To what extent are they replaced by descendants of SFTPC-negative cells during repair after alveolar damage or viral infection? Are SFTPC$^+$ AEC2s a heterogeneous population composed of cells with different capacities for quiescence, proliferation, and differentiation? And finally, what makes up the niche in which AEC2s reside?

Similar questions have been posed for epithelial stem cells in other organ systems such as the skin and gut. In these cases, important insights have come from studies using a combination of in vivo clonal lineage analysis, different injury/repair systems, and in vitro culture of purified cell populations (15–17). Here, we apply similar strategies to epithelial progenitors in the distal lung. For lineage-tracing AEC2s, we have used our *Sftpc-CreER^{T2}* allele (13) in which a cassette encoding tamoxifen-activated (Tmx-activated) CreER is inserted into the endogenous *Sftpc* locus. To assay the reparative behavior of AEC2s, we have used both the bleomycin injury model and a new cell ablation model of alveolar damage in which no fibrosis occurs. We have coupled this model with high-resolution

Conflict of interest: The authors have declared that no conflict of interest exists.

Note regarding evaluation of this manuscript: Manuscripts authored by scientists associated with Duke University, The University of North Carolina at Chapel Hill, Duke-NUS, and the Sanford-Burnham Medical Research Institute are handled not by members of the editorial board but rather by the science editors, who consult with selected external editors and reviewers.

Citation for this article: *J Clin Invest.* 2013;123(7):3025–3036. doi:10.1172/JCI68782.

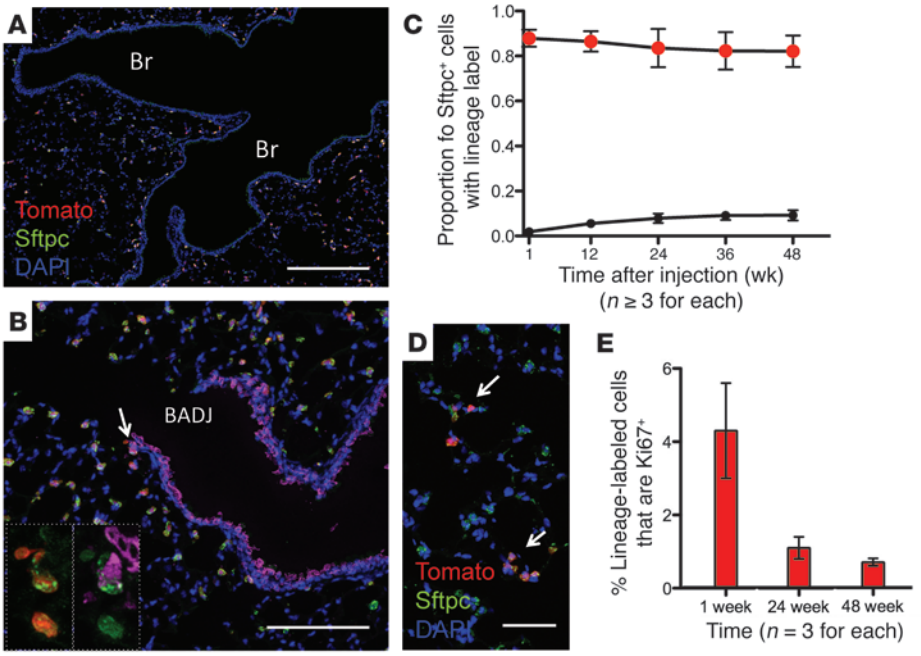

Figure 1

Long term self renewal of SFTPC lineage-labeled alveolar cells. Adult *Sftpc-CreER;Rosa-Tm* mice were dosed ×4 with Tmx (0.2 mg/g). Tiled confocal images of lung sections 4 dpi show (**A**) that all Tm+ cells express SFTPC. The majority locate in alveoli and resemble AEC2s. No label is seen in bronchi/bronchioles (Br), indicating that the *Sftpc-CreER* allele is not active in proximal epithelial precursors in the absence of Tmx. (**B**) Tm+ epithelial cells in the BADJ coexpress SFTPC and SCGB1A1. Insets are high magnifications of cell marked with arrow: Left (Tm, red; SFTPC, green); right (SCGB1A1, purple; SFTPC, green). (**C**) A cohort of 8- to 12-week-old mice was dosed ×2 with 0.25 mg/g Tmx. Controls received vehicle alone. At different dpi, confocal z-stack images of lung sections ($n \geq 3$ mice per point, 6 sections/mouse) were analyzed to give the proportion of SFTPC+ cells with lineage label. This does not significantly decline over the 48-week chase (red circles). Low recombination was seen without Tmx (black circles). (**D**) Section from a 24-week-old Tmx− control mouse from **C** showing small clusters of Tm+ AEC2s (arrows). (**E**) To confirm proliferation of lineage-labeled (Tm+) cells in **C**, sections of lungs ($n = 3$ from Tmx+ group) were stained for Ki67 and percentage of dual positive cells recorded. Error bars indicate mean ± SEM. Scale bars: 250 μm (**A**); 100 μm (**B**); 50 μm (**D**). See also Supplemental Figure 1.

imaging to follow the expansion and fate of AEC2 clones in the repairing lung. Finally, we show for what we believe is the first time that individual lineage-labeled AEC2s can self renew in culture and differentiate into alveolar-like structures ("alveolospheres") that contain both mature AEC2s and cells expressing AECI markers. This is achieved by coculture with a PDGFRA+ mesenchymal population that includes LipidTOX+ lipofibroblasts that normally reside in proximity to AEC2 cells in vivo. We present evidence suggesting that a similar mesenchymal-epithelial dynamic exists between HTII-280+ (18) AEC2s and stromal cells in the human lung.

Results

Sftpc-CreER^{T2} lineage labels AEC2s in the adult lung. To lineage label adult AEC2s, *Sftpc-CreER^{T2};Rosa26R-tdTm* (where *Tm* indicates *Tomato*) double heterozygous mice (abbreviated *Sftpc-CreER;Rosa-Tm*) were given 4 doses of Tmx (0.2 mg/g body weight) and sacrificed at least 4 days after the final injection. As previously reported, this leads to lineage labeling of approximately 85% of SFTPC+ cells (13). Immunohistochemistry, location, and cell morphology confirmed that the great majority (99.5% ± 0.02%) of these cells were AEC2s, while 0.3% ± 0.07% were dual-positive SFTPC+;SCGB1A1+ cuboidal cells in the terminal bronchioles. Very few remaining cells (0.2% ± 0.06%) were SFTPC^{neg};SCGB1A1+ airway cells that were presumably labeled during development (Figure 1, A and B).

AEC2s as a population undergo long-term self renewal and give rise to small clones. To determine whether SFTPC+ AEC2s undergo long-term self renewal in the adult lung, we lineage labeled a population of these cells by injecting a cohort of 8- to 12-week-old *Sftpc-CreER;Rosa-Tm* mice with 2 doses of TMX (0.25 mg/g). We then asked whether the proportion of lineage-labeled SFTPC+ AEC2s remained constant over time or decreased, as would be expected if a non–lineage-labeled population (either SFTPC expressing or not) were to expand preferentially to renew and repair the alveolar epithelium. As shown in Figure 1C, the proportion of lineage-labeled SFTPC+ AEC2s remained constant over the 48-week chase period (87.9% ± 2.7% at 1 week; 86.5% ± 4.5% at 12 weeks; 83.5% ± 8.5% at 24 weeks; 82.3% ± 8.4% at 36 weeks; 82.1 ± 7.0% at 48 weeks; P = NS for all times). We confirmed by Ki67 staining that proliferation of lineage-labeled AEC2s continued throughout the chase (Figure 1E). A few lineage-labeled AEC1s were also seen over time (Supplemental Figure 1A; supplemental material available online with this article; doi:10.1172/JCI68782DS1), supporting the conclusion that AEC2s not only self renew but slowly differentiate during steady-state tissue maintenance.

To test for Tmx-independent recombination of the reporter, a cohort of adult *SftpcCreER;Rosa-Tm* littermates was treated with corn oil vehicle alone. At 12 to 48 weeks, recombination was observed in only a small number of SFTPC+ cells (5%–9%) (Figure 1C). Their low density enabled us to see that lineage-labeled SFTPC+ cells were often present in small clusters (Figure 1D), consistent with a slow rate of self renewal at steady state.

To further explore the clonal expansion of AEC2s, we exploited the *Rosa-Confetti* multicolor lineage-tracing allele (19). Adult *Sftpc-CreER;Rosa-Confetti* double-heterozygous mice ($n = 3$) were injected once with Tmx (0.1 mg/g) to label only a small proportion of AEC2s. After approximately 7 months (30 weeks), small clusters of lineage-labeled AEC2s of like colors were observed (Supplemental Figure 1B), providing strong evidence for clonal proliferation of AEC2s during long-term homeostasis.

SCGB1A1+ cells, but not another Sftpc^{neg} population, contribute to AEC2 replacement after bleomycin injury. Although the proportion of lineage-labeled SFTPC+ AEC2s did not change during steady state, our previous studies and those of others had shown a decline in

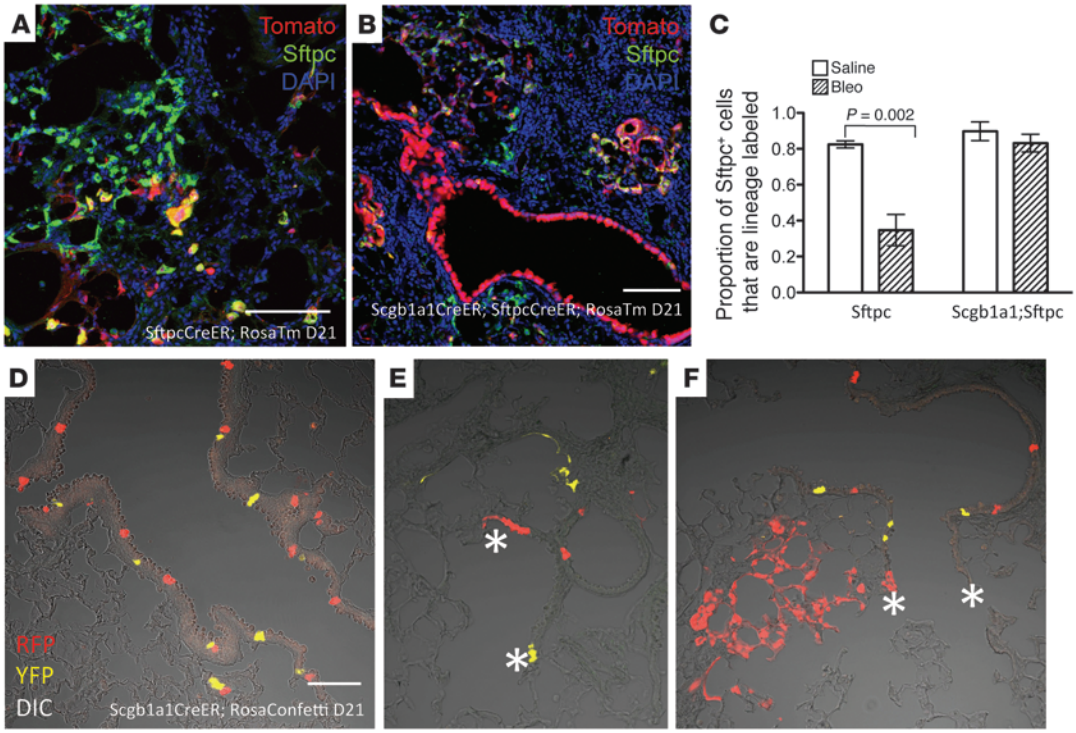

Figure 2

During repair after bleomycin, SCGB1A1 lineage–labeled cells account for most of the SFTPC lineage-negative AEC2s, and clones can arise in bronchioles. *Sftpc-CreER;Rosa-Tm* and *Scgb1a1-CreER;Sftpc-CreER;Rosa-Tm* mice were dosed with Tmx (0.2 mg/g × 4) and exposed to bleomycin (1.25 U/kg). Controls received Tmx and intratracheal saline. Sections of 21-dpi lungs were stained for SFTPC. Confocal z-stack images ($n \geq 3$ mice per point, 6 sections/mouse) were acquired and cells counted from fibrotic areas (high density of DAPI$^+$ nuclei) or from random alveolar areas in controls. (**A**) Fibrotic region of *Sftpc-CreER;Rosa-Tm* lung showing clusters of SFTPC$^+$ AECs that are not lineage labeled. By contrast, in a similar region of *Scgb1a1-CreER;Sftpc-CreER;Rosa-Tm* lung (**B**), significantly more AEC2 cells are lineage labeled. This is quantified in **C**. The smaller decline in value in the *Scgb1a1-CreER;Sftpc-CreER;Rosa-Tm* group compared with *Sftpc-CreER;Rosa-Tm* group suggests that there is no other important source of AEC2 precursors besides SCGB1A1$^+$ cells. (**D**–**F**) *Scgb1a1-CreER;Rosa-Confetti* mice ($n = 3$) were dosed with Tmx (0.05 mg/g × 1) and sacrificed 21 days after bleomycin. Uninjured areas show random labeling of single cells in the bronchiolar epithelium (**D**), while injured areas display clones of labeled cells (**E**) especially in the BADJ (asterisks). (**F**) Clones occasionally extend from the BADJ (asterisks) into the alveoli, suggesting that at least some of the SCGB1A1$^+$ lineage-labeled cells giving rise to AEC2s and AEC1s originate in the bronchioles. Scale bars: 100 μm. See also Supplemental Figure 2.

labeling index after injury of the lung by bleomycin (13, 20). This suggested that a cell type that is negative for SFTPC (or expresses only low levels of the gene) helps to restore the AEC2 population during certain types of lung repair. Potential identities of this progenitor include secretory cells expressing the gene Secretoglobin1a1 (SCGB1A1; CC10; CCSP) in the terminal bronchioles (13, 21–23), cells in the alveoli enriched for integrin $\alpha_6\beta_4$ (20), AEC1 cells, which may proliferate after injury (24), or another as yet unidentified facultative stem cell population.

To address this question, we first confirmed that the proportion of lineage-labeled SFTPC$^+$ AEC2s does indeed decline in fibrotic areas of the lung at 21 days after bleomycin injury (intratracheal delivery of 1.25 U/kg). The control proportion of lineage-labeled SFTPC$^+$ AEC2s in *Sftpc-CreER;Rosa-Tm* mice that received saline is 82.5% ± 2.0% (mean ± SEM; $n = 4$ mice); this proportion declined to 34.7% ± 8.7%; $P = 0.002$ ($n = 4$ mice) in fibrotic areas after bleomycin (Figure 2, A and C).

Previous work has shown that SCGB1A1$^+$ cells can give rise to AEC2s and AEC1s following bleomycin lung injury (21, 23, 25). However, it is not known whether these cells account for all of the SFTPC lineage-negative cells that give rise to AEC2s after bleomycin injury. To specifically address this question, we generated *Sftpc-CreER;Scgb1a-CreER;Rosa-Tm* triple-heterozygous mice and injected them with a high dose of TMX (4 injections of 0.2 mg/g). This strategy labels a majority of AEC2s as well as dual-positive SCGB1A1$^+$;SFTPC$^+$ cells in the bronchoalveolar duct junction (BADJ) and alveoli and SCGB1A1$^+$ secretory cells throughout the bronchioles (Supplemental Figure 2). In control triple-heterozygous mice receiving intratracheal saline but not bleomycin, 89.7% ± 5.2% ($n = 3$ animals) of the SFTPC$^+$ AEC2s were labeled. Importantly, after intratracheal instillation of bleomycin, the proportion of lineage-labeled SFTPC$^+$ cells in heavily fibrotic areas only declined to 83.2% ± 5.0%; P = NS ($n = 5$ mice), a much smaller reduction in the proportion of lineage-labeled AEC2s than was observed in the *Sftpc-CreER;Rosa-Tm* mice (Figure 2, A–C). This result supports the previous observations that *Scgb1a1-CreER* lineage-labeled (referred to as SCGB1A1 lineage) cells give rise to AEC2s after bleomycin injury. The fact that there was still a small decline suggests that some replacement of damaged AEC2 cells by SFTPC^{neg},SCGB1A1^{neg} cells, whether integrin $\alpha_6\beta_4^+$ or not, does occur in this injury/repair system, although the contribution of these cells is only minor.

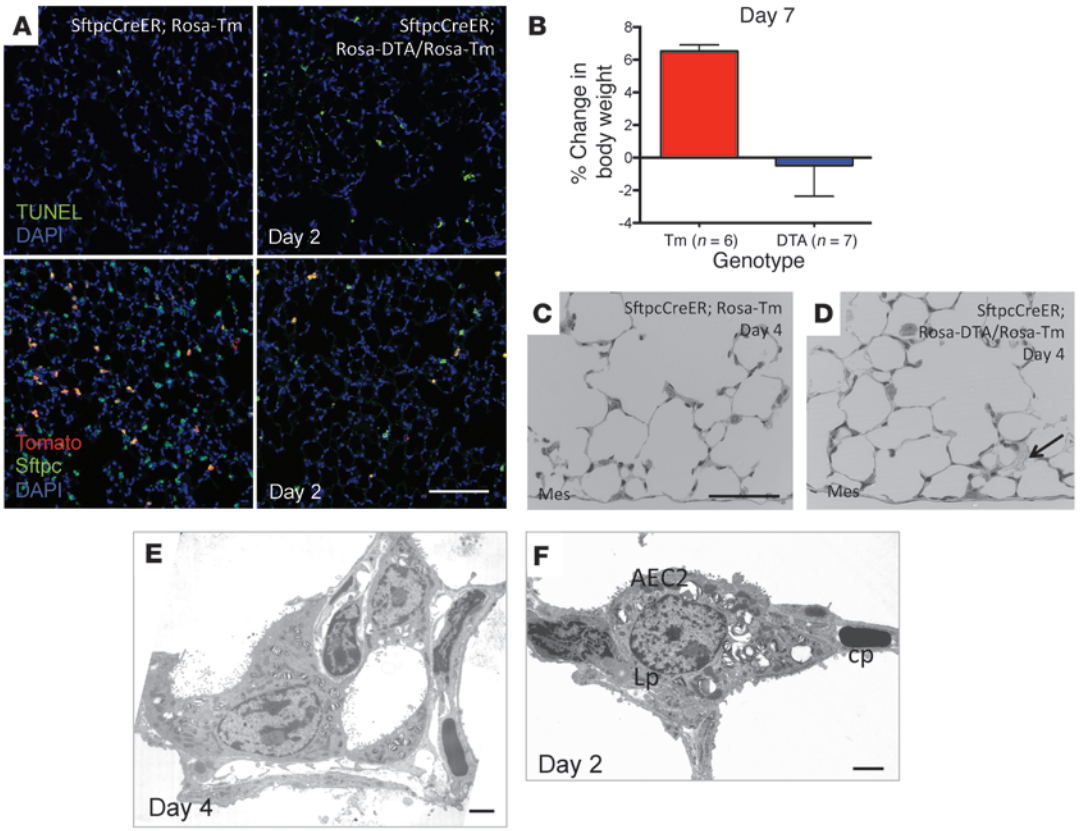

Figure 3

Injury/repair model using *Rosa-DTA* to selectively kill AEC2s in the adult lung. (**A**) *Sftpc-CreER;Rosa-Tm* (left panels) and *Sftpc-CreER;Rosa-DTA/Rosa-Tm* (right panels) mice (at least 8 weeks of age) were given 1 dose of Tmx (0.05 mg/g) and lungs harvested 2 dpi. TUNEL staining shows significant increase in cell death in lungs with *Rosa-DTA* (upper right). Staining for SFTPC (lower panels of **A**) shows that 1 dose of Tmx lineage labels about 52% of the total SFTPC$^+$ AEC2s at 2 dpi. The *Rosa-DTA* allele reduces the number of both SFTPC$^+$ and lineage-labeled cells in the alveoli. (**B**) Loss of AEC2s results in failure of mice to gain weight over a 7-day period after injection. (**C**–**F**) Minimal changes in lung architecture at 2 to 4 dpi. (**C** and **D**) Histology of matched alveolar regions near mesothelium (Mes). At 4 dpi, the overall architecture of *Sftpc-CreER;Rosa-DTA/Rosa-Tm* alveoli (**D**) is very similar to that of controls (**C**), although abnormal AEC2s can be seen (arrow). (**E**) By 4 dpi, small groups of healthy AEC2s are seen in injured lung. (**F**) TEM of lipofibroblast (Lp) adjacent to AEC2 and capillary (cp) at 2 dpi. Scale bars: 100 μm (**A**); 50 μm (**C** and **D**); 2 μm (**E** and **F**). See also Supplemental Figure 3.

The experiments described above used a high dose of Tmx, which labels many cells. This strategy cannot be used to identify the clonal origin of the SCGB1A1 lineage–labeled AEC2s and AEC1s and to determine whether they arise in the bronchiolar epithelium, in the alveoli, or in both locations following bleomycin injury. To address this question, we carried out clonal lineage analysis using *Scgb1a1-CreER;Rosa-Confetti* mice ($n = 3$) given a single low dose of Tmx (0.05 mg/g), which triggers recombination in widely distributed single cells. Mice were sacrificed 21 days after intratracheal bleomycin (1.25 U/kg) and sections analyzed with confocal microscopy for the presence of lineage-labeled clones that span both bronchiolar and alveolar compartments (Figure 2D). In uninjured areas of the lung, single-labeled bronchiolar cells are widely distributed. However, in injured regions (as evidenced by neighboring areas of tissue with a high concentration of DAPI$^+$ nuclei), clones of lineage-labeled bronchiolar epithelial cells are observed in some BADJ regions of all animals, and in some areas the clones extend well into the alveolar region (Figure 2, E and F). These findings strongly suggest that at least some SCGB1A1 lineage–labeled cells present in the bronchiolar epithelium can give rise to AEC2s and AEC1s in a clonal manner.

New model for AEC2-specific alveolar injury and repair with no fibrosis. While intratracheal instillation of bleomycin reliably leads to alveolar injury and repair in mouse lungs, the drug causes injury and/or death to epithelial, endothelial, and some mesenchymal cells and is associated with transient fibrosis. In addition, there is significant disruption of lung architecture, complicating quantitative analysis of cell behavior during repair (14). To avoid these problems, we have developed a more cell-specific injury model compatible with high-resolution imaging. To do this, we generated *Sftpc-CreER;Rosa26R-loxp-GFP-stop-loxp-diphtheria toxin A* (abbreviated *Rosa-DTA*)/*Rosa-Tm* triple heterozygous mice. A single low dose of Tmx (0.05 mg/g) induced expression of the catalytic subunit of diphtheria toxin and triggers cell death in some, but not all, AEC2s. Importantly, by chance, Tmx-induced recombination occurred only at the *Rosa-Tm* locus in a proportion of AEC2s, thereby lineage labeling, but not killing these AEC2s. We could then trace the behavior of these AEC2s following the destruction of their neighbors. We do not expect any bystander effects of DTA expression, as the catalytic subunit alone does not bind at the cell surface (26), and furthermore, murine cells do not express diphtheria toxin receptor (27).

Two days after giving Tmx to *Sftpc-CreER;Rosa-DTA/Rosa-Tm* mice, we observed many TUNEL-positive cells, suggesting apoptosis and cell death (Figure 3A). This was confirmed by transmission electron microscopy (TEM) showing abnormal AEC2s with clumped chromatin and disintegrating organelles as well as cells being engulfed by macrophages (data not shown). We were technically unable to quantify the precise proportion of cell death at this time by costaining for TUNEL and SFTPC. However, while recognizing that Cre-based recombination may not be the same at both Rosa loci, we estimated a value of approximately 52%, based upon the recombination of the *Rosa-Tm* allele with the same dose of Tmx (see below). Immunohistochemistry of tissue from DTA and control animals 2 days after Tmx revealed a significant decrease in the number of SFTPC$^+$ AEC2s after DTA ablation compared with controls (Figure 3A); there was also a similar decrease in the number AEC2s expressing LAMP3$^+$ (DC-LAMP/CD208) — a member of the lysosomal-associated membrane protein family and a marker of normal AEC2s in mouse and human (ref. 28 and Supplemental Figure 3A). Quantitative RT-PCR (qRT-PCR) of whole lung isolated at the same time after Tmx confirmed that the level of transcripts for both AEC2 markers decreased following DTA ablation (Supplemental Figure 3B).

Despite the extent of AEC2 cell death and a transient failure of the mice to gain weight (Figure 3B), the overall histology of the lung remained remarkably intact at 2, 4, 7, and 21 days post injection (dpi) (Figure 3, C and D, and Figure 4): there was little inflammation and no evidence of alveolar collapse. Repair of the epithelium appeared complete by about 21 dpi, as suggested by a normal distribution of SFTPC$^+$ cells in the alveoli (Supplemental Figure 5A). Contrary to what has been described in another injury model in which chronic depletion of AEC2s led to pulmonary fibrosis (29), histology also remained relatively normal even after 4 doses of Tmx (0.05 mg/g) given every 2 weeks, and there was no statistically significant increase in hydroxyproline content (although there was a trend toward significance) in these lungs compared with lungs from *Sftpc-CreER;Rosa-Tm* double-heterozygous controls (Supplemental Figure 3C).

AEC2s undergo clonal proliferation after targeted injury. To lineage trace surviving AEC2s during repair after 1 round of cell ablation, a cohort of *Sftpc-CreER;Rosa-DTA/Rosa-Tm* mice and *Sftpc-CreER;Rosa-Tm* littermate controls were injected with a single dose of Tmx (0.05 mg/g) and lineage-labeled AEC2s followed over 21 days (Figure 4, A–D). As expected from our earlier long-term lineage trace experiments, the proportion of lineage-labeled cells remained relatively constant over the chase period in the *Sftpc-CreER;Rosa-Tm* control lungs (52.1% ± 0.9%, 47.1% ± 5.3%, and 61.4% ± 2.2% at 2 dpi, 7 dpi, and 21 dpi; n = 3 mice per group). In the *Rosa-DTA* group, the initial proportion of lineage-labeled AEC2s was lower, with only 22.9% ± 4.8% of the AECs being tagged at 2 dpi. However, this value also did not change significantly during repair (29.9% ± 3.1%, 7 dpi; 31.5% ± 0.3%, 21 dpi), even as the total number of lineage-labeled AEC2s increased. This suggests that the surviving lineage-labeled cells did not have a proliferative advantage or disadvantage over other survivors that proliferated but were not tagged.

Not unexpectedly, as measured by colocalization of EdU with lineage label at 2 and 7 dpi, there was higher proliferation of AEC2s in *SftpcCreER;Rosa-DTA/Rosa-Tm* mice (8.4% ± 6.8% and 4.3% ± 0.4%, n = 3 mice per group) compared with *SftpcCreER;Rosa-Tm* control animals (0.20% ± 0.19% and 0.31% ± 0.13%). Minimal proliferation was observed in AEC2s of both groups at 21 dpi, consistent with repair being complete around this time (Figure 4, A and C). Confocal analysis of sections of *SftpcCreER;Rosa-DTA/Rosa-Tm* lungs during repair showed initially a preponderance of single lineage-labeled Tm$^+$ cells. A few days later, small clusters were seen; when well separated from each other, these clusters were presumed to represent clones derived from single AEC2s (Figure 4, A and B). The clusters were tightly packed at 2 and 7 dpi. Immunohistochemistry showed that these cells express SFTPC, and in addition, TEM at 4 dpi revealed small groups of morphologically normal AEC2s with lamellar bodies (Figure 3E). Significantly, by 21 dpi, the cells within clusters were more dispersed, sometimes in linear arrays (Figure 4A and Supplemental Figure 4A). Moreover, a few lineage-labeled AEC1s were seen intermingled with lineage-labeled AEC2s at this time (Figure 4A, inset, and Supplemental Figure 4B). Assessment of at least 12 random ×20 fields of view from n = 3 *Sftpc-CreER;Rosa-DTA/Rosa-Tm* animals revealed that 1.3% ± 0.4% of total lineage-labeled cells were AEC1s (compared with 0.30% ± 0.06% in *Sftpc-CreER;Rosa-Tm* control animals). This proportion of lineage-labeled cells scored as AEC1s is in marked contrast to that which we previously observed in *Sftpc-CreER;Rosa-Tm* mice 21 days following bleomycin instillation (41.4% ± 4.4%; ref. 13). All of these data from confocal analysis of sections were recapitulated when whole-mount lung lobes were examined with a multiphoton microscope after clearing in Sca*l*e solution (30), thereby enabling imaging deeper into the tissue (Figure 4B and Supplemental Figure 4C). Together, these results strongly suggest that lineage-labeled AEC2s are capable of clonal proliferation and differentiation during repair after targeted injury.

To further examine clonal proliferation, we used the *Rosa-Confetti* allele. *Sftpc-CreER;Rosa-DTA/Rosa-Confetti* and *SftpcCreER;Rosa-Confetti* controls were given a low dose of Tmx as before and examined at 7, 21, and 70 dpi (n = 1 per group, 2 per group at day 70). Lungs were cleared in Sca*l*e and imaged by whole mount by stereoscopic, confocal, or multiphoton microscopy (Figure 4E and Supplemental Figure 5B). As expected, discrete clones of single colors (either red, green, yellow, or cyan) were randomly dispersed throughout the tissue in *DTA-Confetti* animals. This is again strong evidence that at least a subset of AEC2s are capable of clonal proliferation following injury to the alveolar epithelium.

Because there is much interest in the characterization and potential stem cell role of SFTPC$^+$SCGB1A1$^+$ cells in terminal bronchioles, we sought to determine whether the clones that arose after DTA injury preferentially derived from this cell population. We first quantified the occurrence of SFTPC$^+$SCGB1A1$^+$ cells in the BADJ in the DTA model to determine whether there was an increase in lineage labeling of these cells in the setting of AEC2 ablation. We found an increase in the number of SFTPC$^+$SCGB1A1$^+$ cells in the terminal bronchioles 7 days after DTA ablation when compared with controls (0.93 ± 0.10 dual$^+$ cells per BADJ in DTA animals [n = 3] vs. 0.15 ± 0.04 dual$^+$ cells per BADJ in controls [n = 3]; mean ± SEM; P = 0.002). None of the SFTPC$^+$SCGB1A1$^+$ cells in either experimental group were EdU positive (50 mg/kg dosed 3 hours before sacrifice; data not shown). Furthermore, the occurrence of SFTPC lineage-labeled SFTPC$^+$SCGB1A1$^+$ cells remained very low and was similar between DTA and control animals (0.025 ± 0.013 dual$^+$ cells per BADJ in DTA animals vs. 0.049 ± 0.031 cells per BADJ in controls [n = 3 per group]). The most likely explanation for these findings is that SFTPC is upregulated in SCGB1A1$^+$ cells at the BADJ following injury.

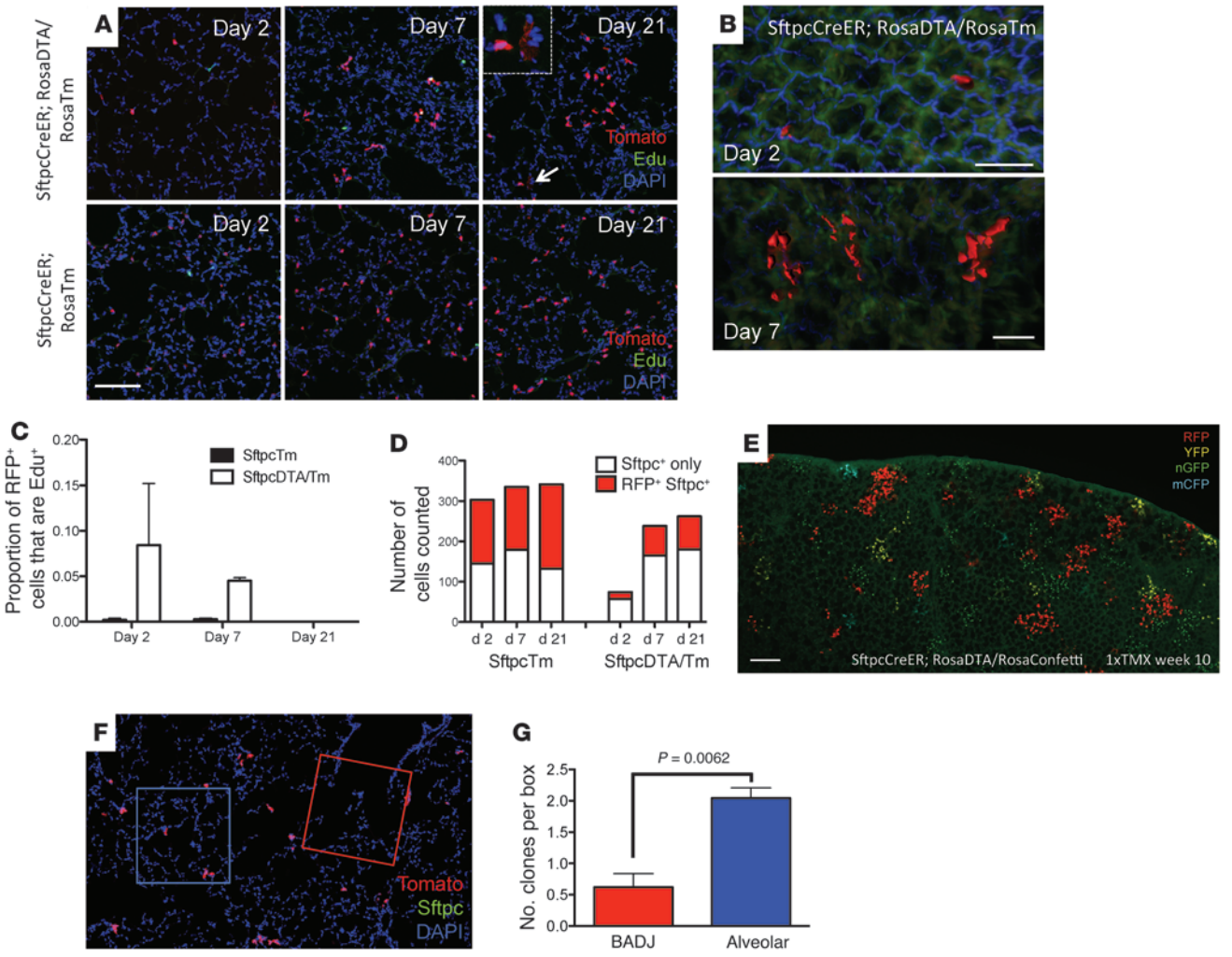

Figure 4

SFTPC$^+$ cells proliferate clonally after targeted AEC2 depletion. (**A**) Lungs from *SftpcCreER;Rosa-DTA/Rosa-Tm* mice (upper panel) were fixed and cleared at different times after Tmx ×1 and 3 hours after EdU. Confocal microscopy shows single-labeled cells at 2 dpi, discrete clones at 7 dpi, and more dispersed clones at 21 dpi. Lineage-labeled AEC1s are present by 21 days (arrow and inset). Controls without Rosa-DTA (lower panels) show no change in Tm$^+$ cells and little EdU labeling. (**B**) Multiphoton images of *SftpcCreER;RosaDTA/Rosa-Tm* lungs at 2 and 7 dpi. (**C**) Decline in EdU labeling index as repair proceeds (n = 3 mice each time). (**D**) To quantify increase in SFTPC$^+$ cells during repair, total SFTPC$^+$ cells within at least 6 random ×20 fields of view (within 2 lobes/mouse) were counted and scored for lineage label. Without injury, values remained constant. With injury, number of SFTPC$^+$ cells increased but proportion of lineage-labeled cells remained the same, suggesting labeled cells do not proliferate preferentially. (**E**) An *Sftpc-CreER;Rosa-DTA/Rosa-Confetti* mouse was given Tmx (0.05 mg/g × 1) and 10 weeks later, lungs were fixed, cleared, and viewed by confocal microscopy. Tiled image shows clones labeled with nuclear GFP (nGFP), cytoplasmic YFP (YFP), membrane cyan (mCFP), and cytoplasmic RFP. (**F** and **G**) Quantification of clone location (representative boxes in **F**) 7 days after Tmx in *Sftpc-CreER;Rosa-DTA/Rosa-Tm* animals suggests that clones do not preferentially arise in or near the BADJ (see text for details). Scale bars: 200 μm (**A**); 50 μm (**B**); 100 μm (**C**). (**F**) Boxes are 300 μm × 300 μm. See also Supplemental Figures 4 and 5.

Following this assessment, we asked whether SFTPC$^+$ cells within or around the BADJ are more likely to clonally proliferate after DTA injury compared with SFTPC$^+$ cells located within the alveoli. To do this, we imaged multiple sections of lungs from n = 3 *Sftpc-CreER;Rosa-DTA/Rosa-Tm* mice 7 days after Tmx injection, along with appropriate littermate controls. For each image, in a blinded manner, we placed a 300 μm × 300 μm square either at the BADJ ($n \geq 25$ BADJs per mouse) or in the alveolar space (removed from the BADJ by at least 300 μm) and counted the number of clones in each square (Figure 4F). If clones preferentially arose from SFTPC$^+$ cells in and around the terminal bronchioles (including dual-positive SFTPC$^+$SCGB1A1$^+$ cells in the BADJ), we would expect to see more clones in the vicinity of the BADJ than in the alveoli. Our analysis revealed the opposite, that there are significantly more clones in the alveolar space than near the BADJ (2.04 ± 0.16 [mean ± SEM] clones per square in the alveoli versus 0.62 ± 0.22 clones per square near the BADJ) (Figure 4G). This result argues that the SFTPC$^+$ cells that clonally expand after DTA injury are not more likely to be in/near the BADJ than within the alveoli. The average number of cells per cluster was similar in each group (2.77 ± 0.17 cells per cluster in DTA group vs. 2.98 ± 0.12 cells per cluster in controls).

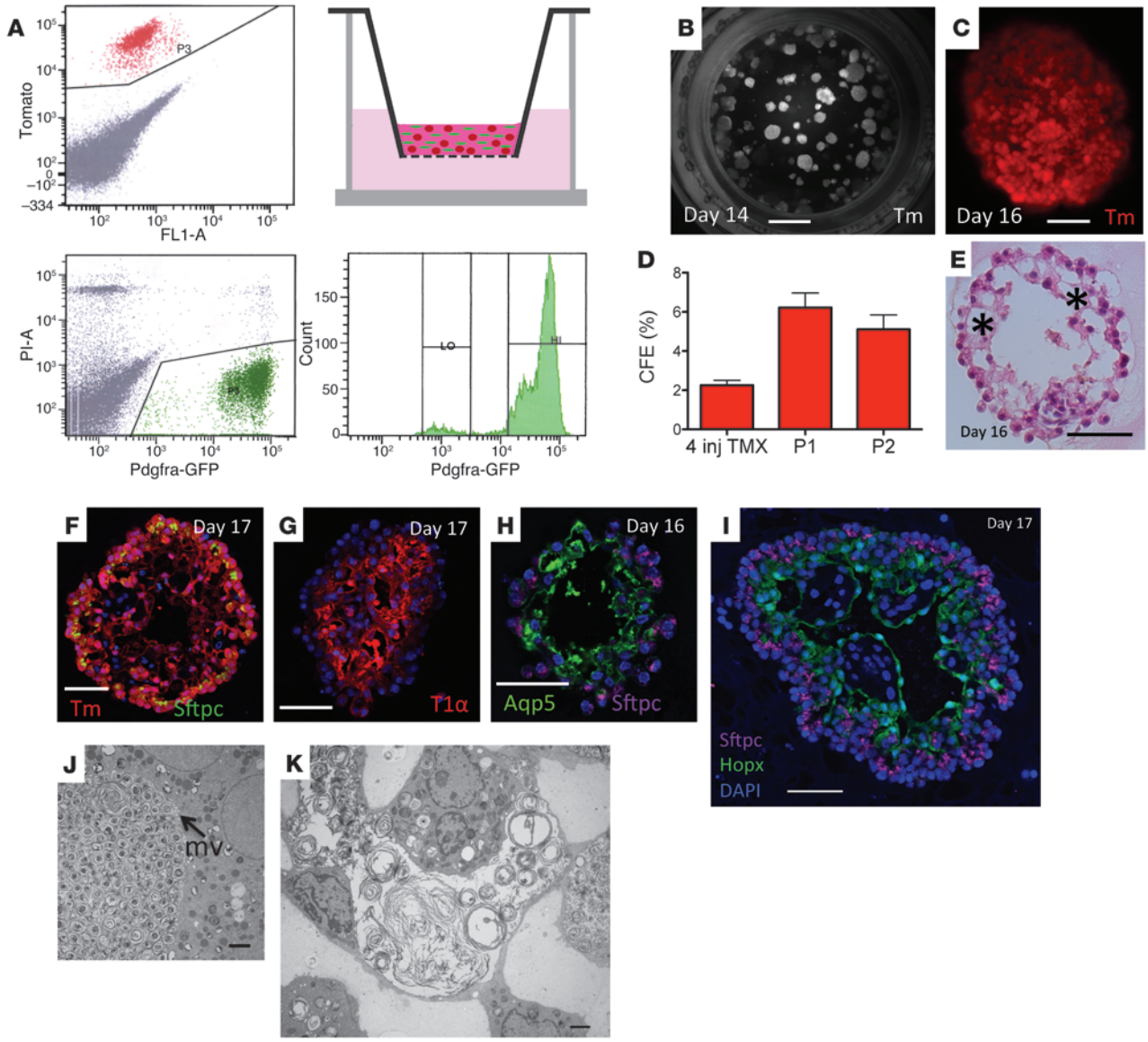

Figure 5

Self renewal and differentiation of AEC2 cells in 3D organoid culture. (**A**) *Sftpc-CreER;Rosa-Tm* mice were dosed ×4 with Tmx (0.2 mg/g) and at least 4 dpi lungs were dissociated and sorted by FACS. The Tm$^+$ fraction (P3, top left) was seeded at a density of 5,000 cells in 90 μl of 50% Matrigel in a 24-well Transwell insert (top right) together with 1 × 10^6 PDGFRA-GFP^{hi} stromal cells freshly sorted from lungs of a *Pdgfra-H2B:GFP* transgenic mouse (P3, bottom panels). (**B** and **C**) After 14 days, spheres of lineage-labeled cells are present in various sizes. (**D**) CFE is 2.3% ± 0.3% for primary cultures (n = 8 experiments, ≥ 2 replicates per experiment), 6.2% ± 0.7% after passage 1, and 5.1% ± 0.7% after passage 2. (**E**–**I**) Histology and immunohistochemistry of sections of spheres after 16–17 days shows (**E**) alveolus-like areas (asterisk) with more elongated cells, (**F**) that all cells are lineage labeled and those on the periphery express SFTPC, while cells in the interior express T1a, AQAPORIN 5 (Aqp5) (**G** and **H**), and HOPX (**I**) — markers of AEC1s (see also Supplemental Figure 7). (**J** and **K**) TEM of spheres at day 16 shows many cells with lamellar bodies at different stages of maturation and apical membranes with dense microvilli (mv). The cells release surfactant into the interior of the spheres where it accumulates in large amounts. Scale bars: 100 μm (**B**); 50 μm (**C**); 50 μm (**E**); 50 μm (**F**–**I**); 2 μm (**J** and **K**). See also Supplemental Figures 6 and 7.

In order to rule out spontaneously occurring recombination events early in development as the etiology of the clonal AEC2s, we sacrificed a cohort of adult *Sftpc-CreER;Rosa-DTA/Rosa-Confetti* mice (n = 3), and imaged cleared lung tissue on the stereoscope. We saw no evidence of spontaneously occurring lineage-labeled AEC2 clusters (Supplemental Figure 3D).

Single lineage-labeled AEC2s form 3D alveolar-like structures (alveolospheres) when cultured with PDGFRA-H2B:GFP$^+$ stromal cells. The results of the in vivo injury/repair model described above show that individual SFTPC$^+$ AEC2s can clonally proliferate and give rise to AEC1s in vivo in the context of a preexisting alveolar environment, albeit one that has been specifically depleted of AEC2s. This suggests that components of the niche survive the injury, but precisely which cells, signals, and/or matrix components are important for regulating clonal expansion is not known. To begin to address these questions, we established a clonal 3D coculture system in which AEC2s were

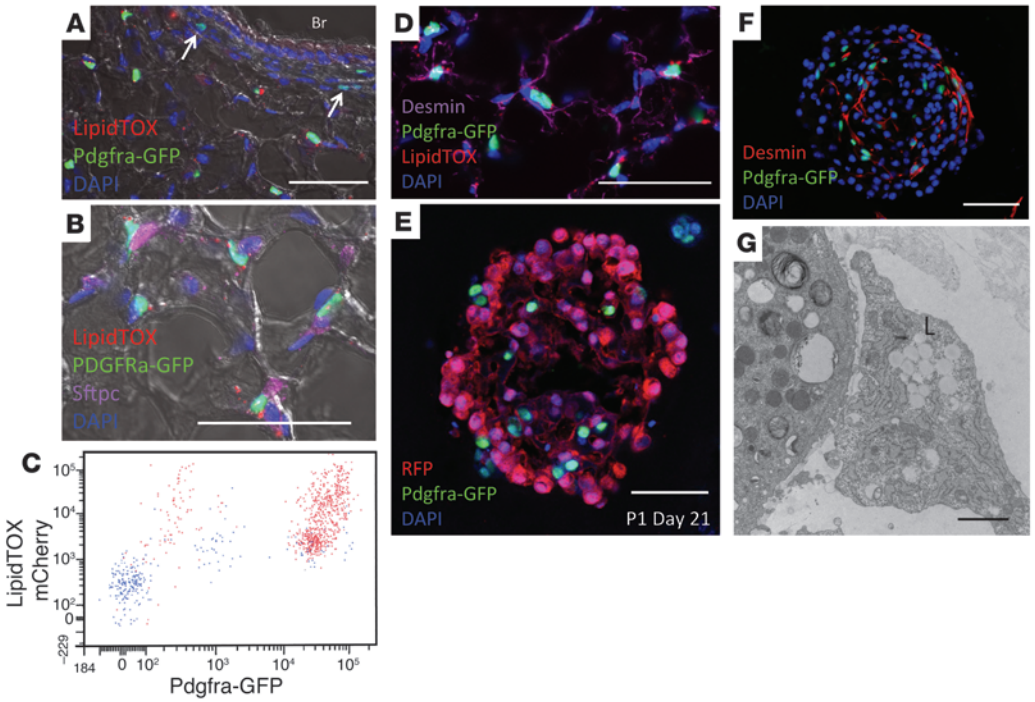

Figure 6
Recapitulating the AEC2 stem cell niche. Sections from adult *Pdgfra-H2B:GFP* lungs were stained for neutral lipid and/or SFTPC. (**A**) LipidTOX staining colocalizes with high-intensity GFP$^+$ cells in alveoli, but not with lower-intensity GFP$^+$ cells (arrows) in the bronchiolar wall. (**B**) LipidTOX$^+$, PDGFRA-GFP$^+$ cells are closely apposed to SFTPC$^+$ AEC2s (purple). (**C**) FACS-sorted PDGFRA-GFP^{hi} cells are also positive for LipidTOX. (**D**) LipidTox$^+$ PDGFRA-GFP$^+$ cells express the intermediate filament protein desmin. (**E** and **F**) Multiple PDGFRA-GFP$^+$;desmin$^+$ cells are interspersed throughout an alveolosphere at day 21. (**G**) TEM of alveolosphere reveals multiple lipid-filled cells (L) adjacent to lamellar body–containing AEC2s. Scale bars: 50 μm (**A**–**F**); 2 μm (**G**).

combined with specific mesenchymal cell populations. Lineage-labeled AEC2s from *Sftpc-CreER;Rosa-Tm* animals that received doses of Tmx that labeled 85% of AEC2s were isolated by FACS and seeded in culture medium with 50% Matrigel in Transwell inserts (Figure 5A). Importantly, when plated alone under these conditions, there was no proliferation of the lineage-labeled cells.

Recognizing the importance of PDGFRA$^+$ cells in lung development and alveolarization (31), we cocultured AEC2s with primary PDGFRA$^+$ cells isolated from heterozygous *Pdgfra-H2B:GFP*$^+$ animals (6 to 12 weeks of age). In these mice, H2B:GFP is expressed from the endogenous *Pdgfra* locus (32), and approximately 29% of the total mesenchymal cell population in the lung is *Pdgfra-H2B:GFP*$^+$ (Supplemental Figure 6A). We collected GFP^{hi} cells (Figure 5A), a population that is thought to include alveolar fibroblasts and lipofibroblasts (33), and seeded them with lineage-labeled AEC2s at a density of 5,000 AEC2s and 100,000 GFP^{hi} cells per insert. Sphere-like colony formation was typically seen by 4 to 6 days post plating (dpp). Spheres enlarged for the first 10 days and appeared to have a single lumen; they later become denser as cells accumulated within the center (Figure 5, B and C). Colony forming efficiency (CFE) at 14 dpp was 2.3% ± 0.3% (mean ± SEM) (n = 8 experiments, ≥ 2 technical replicates per experiment) (Figure 5D). The clonal origin of spheres was confirmed by mixing experiments in which lineage-labeled AEC2s were plated at equal densities with GFP^{hi} cells sorted from a *Sftpc-GFP* transgenic mouse line (34). All resulting spheres were either completely Tm$^+$ or GFP$^+$ (Supplemental Figure 6, C and D).

Histological analysis and confocal microscopy (Figure 5, E–H) showed that all the epithelial cells within spheres were lineage labeled. Markedly, the peripheral cells were cuboidal, expressed SFTPC (but not SCGB1A1), and proliferated as judged by Ki67 staining (Supplemental Figure 6B). Interior cells were more elongated and expressed the AEC1 markers T1a (Pdpn) and Aquaporin 5 (Aqp5). Most of these cells also expressed homeodomain only protein x (HOPX) (Figure 5I), a new marker for AEC1s in the mouse lung. We initially identified *HopX* in studies comparing transcripts in SFTPC lineage-labeled cells at different times after bleomycin injury to identify potential markers or regulators of AEC2 differentiation (ref. 13 and our unpublished observations). HOPX is known to regulate both cardiac development (35) and pulmonary maturation (36) and immunohistochemistry of adult mouse lungs showed HOPX expression in AEC1s (Supplemental Figure 7).

All lineage-labeled spheres were of the morphology described above (serial sections of at least 50 spheres fixed after 14–17 days in culture from n = 3 independent experiments) and none contained SOX2$^+$, SCGB1A1$^+$, KRT5$^+$, or p63$^+$ secretory or basal cells (data not shown). This uniformity is in marked contrast to the multiple colony types described by other investigators in which distal lung cells, sorted by surface marker expression, are plated in 3D Matrigel assays (25, 37, 38).

TEM was used to investigate the phenotype of Sftpc-CreEr lineage-labeled cells in 3D culture. This showed that by 14 dpp, many cells had abundant, well-formed lamellar bodies containing surfactant. Moreover, the contents were clearly being released into the inner spaces of the spheres, where they accumulated in copious amounts. The elongated cells lacked lamellar bodies but had thin cytoplasmic projections, consistent with the morphology of AEC1s (Figure 5, J and K). Given that colonies arising from individual AEC2s have an alveolar-like structure and contain cells that resemble both mature AEC2s and AEC1s, we have termed them "alveolospheres."

To determine whether lineage-labeled AEC2s continue to self renew and differentiate in culture, 14 dpp spheres were dissociated and single Tm$^+$ cells isolated by FACS and replated with freshly isolated PDGFRA-GFP^{hi} cells. CFE was 6.2% ± 0.7% after passage 1 and 5.1% ± 0.7% after passage 2 (P = NS for P1 vs. P2) (Figure 5D). Moreover, colonies had the same expanded morphology, with

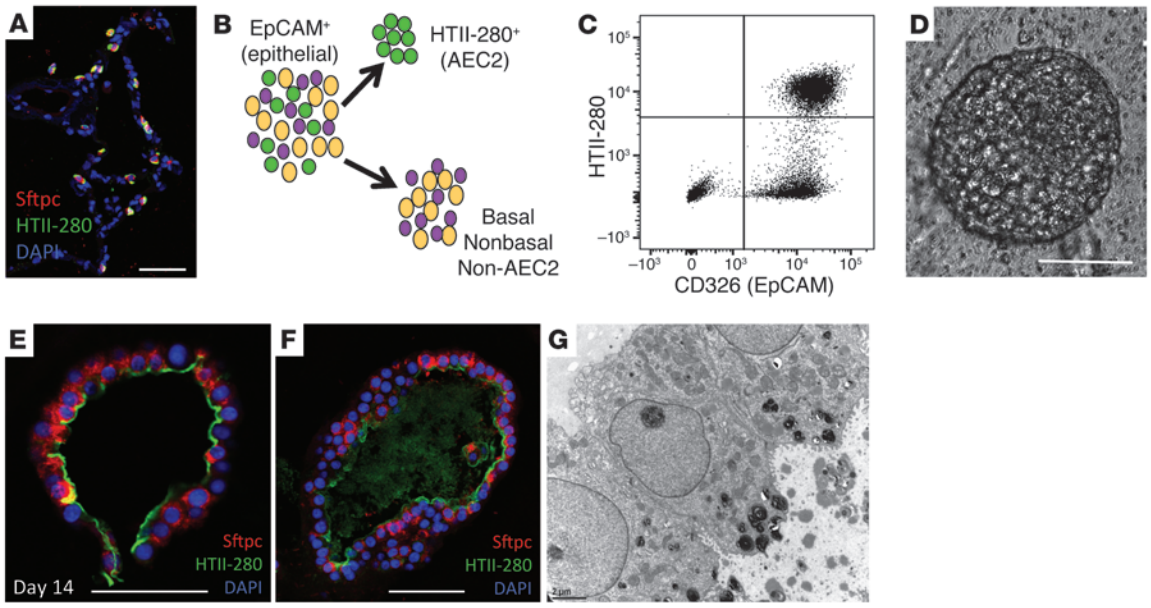

Figure 7
Human AEC2s form self-renewing colonies in 3D organoid culture. (**A**) Immunohistochemistry of human lung sections for SFTPC and HTII-280 shows colocalization of the 2 AEC2 markers. (**B** and **C**) Sorting strategy and representative flow plot. (**D**) Representative sphere at day 14. (**E** and **F**) Immunohistochemistry of human spheres at day 14 showing luminal HTII-280 staining and variable SFTPC staining. (**G**) TEM of a sphere derived from a single HTII-280+ cell (passage 1) showing lamellar bodies and microvilli on the luminal surface. Scale bars: 50 μm (**A**); 100 μm (**D**); 50 μm (**E** and **F**); 2 μm (**G**).

SFTPC+ cells on the periphery and cells with AEC1 markers inside (data not shown).

Recapitulating the AEC2 stem cell niche with Pdgfra-H2B:GFP+ cells. To address the specificity of the PDGFRA+ trophic effect, we seeded AEC2s with fibroblasts from an immortalized fibroblast cell line (MLg neonatal mouse lung fibroblasts) previously shown to support the growth of distal mouse lung epithelial progenitor cells (37, 39). Under these conditions, CFE between days 11 and 14 was only 1.5% ± 0.2% (n = 3 experiments). While there was some evidence of differentiation of AEC2s to T1a+ AEC1s after 14 days in culture, the colonies were much smaller and flatter than those grown with PDGFRA+ cells (Supplemental Figure 6E).

The observation that PDGFRA-GFPhi cells efficiently promote the self renewal and differentiation of isolated SFTPC+ AEC2s in culture suggests that these mesenchymal cells constitute a critical component of the AEC2 stem cell niche in vivo. Lung sections from normal *Pdgfra-H2B:GFP* mice showed that SFTPC+ AEC2s are generally located in close proximity to cells expressing high levels of PDGFRA-GFP fluorescence (PDGFRA-GFP+) (Figure 6B). The PDGFRA-GFP+ cells expressed the intermediate filament protein desmin (Figure 6D and ref. 40), while our previous studies showed that they do not coexpress PDGFRβ or αSMA (13). There are PDGFRA-GFP+ cells near the aSMA+ airways, but these cells appeared to express H2B:GFP at lower levels than in the alveoli (Figure 6A). LipidTOX staining revealed that the majority of PDGFRA-GFP+ cells in the alveoli contained lipid droplets (Figure 6, A and B) and PDGFRA-GFP+ cells were LipidTOX+ when FACS-sorted (Figure 6C), evidence supporting the conclusion that these PDGFRA-GFP+ cells are lipofibroblasts (41). TEM analysis of a normal area from *Sftpc-CreER;Rosa-Tm/Rosa-DTA* lung at 2 dpi (Figure 3F) confirmed previous studies showing lipofibroblasts in close proximity to AEC2s in vivo (40). In addition, immunohistochemistry confirmed the presence of PDGFRA-GFP+ cells within and around the spheres, and TEM of alveolospheres revealed lipid-filled cells in close proximity to the lamellar body–containing cells (Figure 6, E–G).

Human AEC2s form self-renewing colonies in 3D culture. We have begun to address the question of whether AEC2s from human lungs are also long-term self-renewing stem cells able to give rise to alveolospheres in 3D culture. AEC2s were isolated using FACS based on expression of the surface marker HTII-280 (18). Immunohistochemistry of normal human lungs confirmed that HTII-280 and SFTPC colocalize, with HTII-280 being expressed on the luminal surface and SFTPC in the cytoplasm (Figure 7A). There was no evidence of HTII-280 staining in the airways except for occasional cuboidal cells in respiratory bronchioles.

To establish 3D culture, HTII-280+ cells isolated by FACS were seeded in Transwell inserts in 50% Matrigel with MRC5 cells, a fetal human lung fibroblast cell line. Spheres were seen after 5–7 days with a CFE of 4.2% ± 0.8% (n = 3 biological replicates; mean ± SEM) (Figure 7, B–D). No spheres were observed in the absence of MRC5 cells. Serial subculture resulted in CFEs of 7.4% ± 1.6% and 4.9% at passages 1 and 2, respectively (n = 3 at passage 1; n = 2 at passage 2). Histological analysis showed that the human spheres were composed of a single epithelial layer; all cells express HTII-280 on the luminal surface, and a majority, but not all, express SFTPC. TEM reveals the presence of lamellar bodies, consistent with at least some of the cells being mature AEC2s (Figure 7, E–G). No cells in the spheres morphologically resemble or express AEC1 markers.

Discussion

Important goals for the field of lung stem cell research are to define the epithelial populations that maintain the alveolar region

and repair it after injury and to identify the signaling pathways that regulate these behaviors. Here, we have addressed some outstanding questions and opened up new opportunities for future advances. Specifically, we provide evidence that SFTPC$^+$ AEC2s, as a population, function as alveolar progenitors and long-term stem cells in the adult lung. This evidence comes from lineage-tracing studies both during homeostasis and in a model of alveolar repair that allows us to visualize in situ clonal expansion of individual AEC2s. Finally, our new alveolosphere assay shows that a population of *Pdgfra-H2B:GFP^{hi}* stromal cells, which includes lipofibroblasts that normally reside in the proximity of AEC2s, can support their clonal growth and differentiation in vitro.

Our previous lineage-tracing experiments had established that SFTPC$^+$ AEC2s can proliferate and give rise to AEC1s in vivo (13). What was missing was evidence that the same SFTPC$^+$ cells can maintain the AEC2 population over the long term, an important criterion for defining the population as containing stem cells. We now show that long-term self renewal does occur, at least over almost a year. In the unperturbed lung, lineage-labeled AEC2s give rise to only small clones of daughter cells, and there is a low rate of differentiation into AEC1s. However, clonal growth and differentiation are both enhanced if the number of AEC2s is depleted by selective cell ablation. Interestingly, while AEC2s do give rise to AECIs during DTA-induced repair, the rate of differentiation still appears to be significantly lower than during repair after bleomycin-induced lung injury (13). This suggests that bleomycin injury promotes the production of local signals that enhance the conversion of AEC2s to AEC1s. In the future, clues as to the identity of these signaling pathways may come from comparing the transcriptional activities of AEC2s and stromal cells in the 2 injury/repair models.

While SFTPC$^+$ AEC2s can maintain the alveoli during steady state and after depletion of AEC2s, other epithelial cell populations clearly contribute to alveolar repair following bleomycin-induced injury. We and others have previously shown that in the bleomycin model, epithelial cells that express SCGB1A1 can proliferate and differentiate into AEC2s (13, 21, 23). It has been suggested that other SFTPC^{neg} cells, including those enriched for integrin $\alpha_6\beta_4$ (20), are mobilized to give rise to AEC2s under conditions of severe injury and inflammation. However, our studies following the populations of cells lineage labeled by both *Sftpc-CreER* and *Scgb1a1-CreER* alleles in fibrotic regions of the bleomycin-treated lung suggest that any contribution of SFTPC^{neg} cells to the repair is only a minor one. Our AEC2 cell–specific ablation model of alveolar injury has opened the possibility of using clonal analysis to follow AEC2 localization and behavior during the 21-day repair period. Immediately after AEC2 depletion, only single lineage-labeled cells were seen. These gave rise to clusters of cells that likely represent clones. These clusters were not preferentially localized to the BADJs, but were found throughout the alveoli. They were closely packed at 7 dpi, but by 21 dpi were more widely distributed beyond the diameter of a typical alveolus. Two explanations for this apparent dispersal are the expansion of portions of the lung that collapsed following loss of AEC2s and active migration of SFTPC$^+$ cells themselves. Currently, we favor the latter hypothesis because collapse appears to be minimal and expansion would not account for the linear arrays of lineage-labeled cells seen at 7 and 21 dpi. We hypothesize that the cells travel through fenestrations in the alveoli known as pores of Kohn (42, 43) and disperse within an individual acinus, which is composed of hundreds of alveoli. Future studies will use live imaging to address the question of AEC2 migratory behavior. It will also be important to carry out statistical analysis of changes in clone size over time under different conditions, as done recently in other organ systems (17, 44). This will give critical insight into the heterogeneity of the AEC2 population in vivo and whether some cells behave as committed progenitors during repair while others behave as long-term stem cells.

The fact that we have been able to grow and serially subculture individual AEC2s in a 3D organoid culture system supports the concept that SFTPC$^+$ AEC2s as a population contain stem cells. We are confident that alveolospheres are not derived from SFTPC$^+$;SCGB1A1$^+$ cells in the terminal bronchioles because these cells make up only a small percentage of the total lineage-labeled population (0.29%) and the CFE in our assay is consistently about 10-fold higher. We cannot exclude, however, that a subset of AEC2s within the alveoli is more capable of clonal growth in vitro than others; further quantitative analysis is needed to address this interesting question.

Importantly, while there was some variation in size of lineage-labeled spheres in culture, they displayed the same morphology after serial sectioning. They consistently and reproducibly contained not only well-differentiated AEC2s with mature lamellar bodies but also cells localized to the interior of the spheres that express multiple AECI markers, including HOPX, but not bronchiolar cell types. This homogeneity demonstrates an important characteristic of our culture system: that we are starting with a well-characterized, specific population of cells known to initially reside in the alveoli that gives rise to a homogenous population of colonies containing only alveolar cells. This is in contrast to the populations of distal progenitor cells studied by other investigators that ultimately yield mixed colony types containing both alveolar and bronchiolar cells (25, 37, 38).

The alveolosphere assay we describe here has opened up strategies for identifying the cells that make up the niche of AEC2s in vivo and the signals that they produce. The *Pdgfra-H2B:GFP^{hi}* population, which appears to contain alveolar fibroblasts and lipofibroblasts, is clearly able to support both the proliferation and differentiation of AEC2s. However, we do not know whether these properties are shared by all cells in the GFP$^+$ population or whether some subsets of cells are efficient at supporting proliferation while others promote conversion of AEC2s into AEC1s. The relatively low CFE in our assay, even in the presence of PDGFRA$^+$ cells, suggests that there are other crucial components of the niche, for example, endothelial cells or even AEC1s, that need to be added for optimal clonal expansion.

Finally, our data show that human AEC2s are capable of clonal growth in vitro, but we have not observed the differentiation of these AEC2s into AEC1s. One potential reason for this deficiency is that MRC5 cells do not adequately recapitulate the human alveolar stem cell niche in this model. Interestingly, hyperplastic AEC2s and accelerated cell proliferation are common features of IPF (45), suggesting that dysregulation of the alveolar niche may be an important mechanism in pathological remodeling of the lung parenchyma. Future experiments will test the hypothesis that stromal cells are critical regulators of alveolar homeostasis and are dysregulated in tissue remodeling.

Methods

Mice. Mice were *Sftpc-CreER^{T2}*; *Scgb1a1-CreER^{TM}*; and *Rosa26R-CAG-tdTm (Rosa-Tm)* (13); *Rosa26R-CAG-Confetti (Rosa-Confetti)* (19) (supplied by

Hans Clevers); *Rosa26R-loxp-GFP-stop-loxp-DTA (Rosa-DTA)* and B6.129S4-*Pdgfra*$^{tm11(EGFP)Sor}$/J *(Pdgfra-H2B:GFP)* from The Jackson Laboratory and *Sftpc-GFP* (34). Mice for the 48-week lineage trace were on a 129S;C57BL/6 mixed background and controls matched for sex and were littermates. All other mice were at least at the N2 backcross generation to C57BL/6. Most mice were 8–12 weeks old; *Pdgfra-H2B:GFP* mice were at least 6 weeks old. There was some variability in the extent of injury following TMX dosing (0.05 mg/g) of *Sftpc-CreER;Rosa-DTA/Rosa-Tm* mice, as approximately 20% of injected mice died between 4 and 6 dpi with no apparent sex differences. Administration of Tmx at doses higher than 0.05 mg/g led to substantial animal mortality.

Tmx, bleomycin, and EdU administration. Tmx (T5648; Sigma-Aldrich) was a 20 mg/ml stock solution in corn oil and given via i.p. injection. Bleomycin (1.25 U/kg in 0.9% sterile saline) was administered intratracheally as described (13). EdU (Click-iT EdU Alexa Fluor 647 Imaging Kit C10340; Invitrogen) was administered via i.p. injection (50 mg/kg).

Histology and immunohistochemistry. Mouse tissue was routinely fixed with 4% PFA in PBS and cryosections (12 μm) and paraffin sections (7 μm) prepared as described (13). Paraffin sections underwent 10 mM sodium citrate antigen retrieval. Antibodies were as follows: rabbit, SFTPC (1:500; #ab3786; Millipore); goat, SFTPC (1:100; #SC-7706; Santa Cruz Biotechnology Inc.); goat, secretoglobin 1a1 (SCGB1A1) (1:10,000; Barry Stripp); rabbit, aquaporin 5 (1:200; #ab78486; Abcam); hamster, Pdpn (T1α) (1:1000; clone 8.1.1; DSHB); rabbit, HOPX (1:250; #SC-30216; Santa Cruz Biotechnology Inc.); chicken, GFP (1:1000; #GFP1020; Aves Lab); rabbit, RFP (1:250; #600–401379; Rockland); rabbit, desmin (1:200; #RB-9014-P0; Thermo-Fisher); rabbit, Ki67 (1:500; #ab15580; Abcam); rat, Lamp3 (1:50; #DDX0192; Dendritics); rabbit, Sox2 (1:750; #WRAB-1236; Seven Hills Bioreagents); rabbit, Krt5 (1:1000; #PRB-160P; Covance); and mouse, p63 (1:50; #SC-8431; Santa Cruz Biotechnology Inc.). Alexa Fluor–coupled secondary antibodies (Invitrogen) were used at 1:500. TUNEL (Roche Applied Science) and HCS LipidTOX (Life Technologies) staining were performed on paraffin or cryosections respectively, according to the manufacturers' instructions. EdU staining was performed according to the manufacturer's instructions. Human tissue and colonies were fixed in 10% neutral buffered formalin overnight and then placed in PBS until paraffin embedding. Mouse IgM anti-human HTII-280 (1:100 dilution of hybridoma supernatant) was generously provided by Leland Dobbs (Cardiovascular Research Institute, UCSD, San Francisco, California, USA) (18).

qRT-PCR. Gene expression levels were quantified by qRT-PCR on the StepOne Plus Real-Time PCR System (Applied Biosystems) as described previously (13). Primers are listed in Supplemental Table 1.

Mouse lung dissociation and FACS. Lungs were dissociated with a protease solution as described (13). Whole-lung suspension was blocked in 1% FcX TruStain (#101320; Biolegend) in 2% FBS, 2% BSA in 1× PBS. Antibodies for mouse flow cytometry were optimized with appropriate IgG isotype controls and were as follows: rat, CD31-biotinylated (1:50, #13-0311; eBioscience); rat, CD45-biotinylated (1:200; #13-0451-82; eBioscience); and rat, EpCAM-PE/Cy7 (1:800, #25-5791-80; eBioscience). Secondary antibody was as follows: PE/Cy5 streptavidin (1:500, #405205; Biolegend). Sorting was performed on FACS Vantage SE, and data were analyzed with FACS Diva (BD Biosciences).

Confocal microscopy. All images used for scoring cells consisted of a Z stack of multiple optical sections captured on a Zeiss 710 or Zeiss 780 inverted confocal microscope. Confocal Z stack images were analyzed and all cells counted with the Manually Count Object feature on MetaMorph (Version 7.7.1.0).

Scale processing and imaging. Sca*l*e A2 reagent (30) (4M urea [Fisher BP169-212], 0.1% wt/vol Triton X-100, 10% wt/wt glycerol in water) was allowed to stand for at least 1 day at room temperature before use. Following fixation with 4% PFA and washing with PBS, tissue was transferred to Sca*l*e A2 and kept on a rocker at 4°C for 1–2 weeks until maximal tissue clearing occurred. Whole-mount samples were imaged either on the inverted Zeiss 710 confocal microscope in a 35-mm glass-bottom microwell dish with a 10× objective or immersed in Sca*l*e A2 solution using an Olympus FV1000 Multiphoton scope equipped with a ×25/0.9 NA ScaleView immersion lens (XLPLN25XSVMP WD 8 mm) and Prior H117 ProScan III encoded XY motorized stage, allowing acquisition of tiled images from large areas and volumes of tissue. Imaris software was used to reconstruct and analyze 3D images acquired from the multiphoton scope.

Hydroxyproline assay. Total lung collagen content was measured by the hydroxyproline method (46).

TEM. Tissue and cell culture insert were processed to preserve lamellar bodies as previously reported (47).

Mouse cell culture. Sorted cells were resuspended in MTEC/Plus (48), and mixed with 1:1 growth factor–reduced Matrigel (BD Biosciences); 90 μl was placed in a 24-well 0.4-μm Transwell insert (Falcon). 5×10^3 AEC2s and 1×10^5 PDGFRA-GFP^{hi} cells were seeded in each insert. 500 μl MTEC/Plus was placed in the lower chamber, and medium was changed every other day. ROCK inhibitor (10 μM, Y0503; Sigma-Aldrich) was included in the medium for the first 2 days of culture, which was at 37°C in 5% CO_2/air. For paraffin embedding, the Matrigel disc was removed, dehydrated through ethanol, and transitioned into paraffin by standard protocols.

For passaging experiments, spheres were dissociated from Matrigel with the addition of 60 μl Dispase (catalog #354235, 5 U/ml; BD Biosciences) to the insert and incubation at 37°C for 30 minutes. Cells were washed and then incubated in 0.05% Trypsin-EDTA for 30 minutes at 37°C to create a single-cell suspension. Cells were then sorted via FACS, and Tm$^+$ cells were replated with primary PDGFRA-GFP$^+$ cells.

Human cell culture. Under IRB-approved protocols, human AEC2s were isolated from lungs not used for transplantation. Parenchyma was mechanically dissociated by mincing and further dissociated using 2 U/ml dispase (BD Biosciences), 0.25% trypsin/2 mM EDTA (Cellgro), and 10 U/ml elastase (Worthington). Dissociated cells were passed through a 70-μm cell strainer and plated onto PurCol-coated (Advanced Biomatrix) culture dishes in bronchial epithelial growth medium (BEGM) (49) overnight at 37°C. The following day, adherent cells were harvested using trypsin/EDTA and labeled for FACS using PE/Cy7 mouse anti-CD45 (0.6 μg/ml 304015; BioLegend), Alexa Fluor 647 anti-EpCAM (0.6 μg/ml 324212; BioLegend), PE/Cy7 anti-CD31 (0.6 μg/ml 303117; BioLegend), mouse IgM anti-human HTII-280 (1:60 dilution), and Alexa Fluor 488 goat anti-mouse IgM (20 μg/ml A-21042; Invitrogen). Single viable cells that were CD45$^-$, CD31$^-$, EpCAM$^+$, and HTII-280$^+$ were mixed with MRC5 fibroblasts in 1:1 Matrigel/human ALI medium (49) and 100 μl added to 24-well (0.4-μm) Transwell filter inserts (Greiner Bio-One). 500 μl of ALI medium was placed in the lower chamber and changed every other day. Cultures were maintained in a humidified 37°C incubator in 5% CO_2/air.

Statistics. All results are mean ± SEM. All error bars on graphs represent SEM. Statistical tests are 2-tailed *t* tests. $P \leq 0.05$ was considered statistically significant.

Study approval. Mouse experiments were performed under IACUC guidelines and approved protocols at Duke University. Human lung epithelial cells were isolated under protocols approved by the Institutional Review Boards at both Duke University and University of North Carolina at Chapel Hill.

Acknowledgments

We thank the Duke University Light Microscopy Core Facility for assistance with imaging and Kimberlie Burns, Cystic Fibrosis Center Histology Core, UNC, Chapel Hill for assistance with TEM, and Lynn Sakai, Terry Lechler and other colleagues for stimulating discussions. This work was supported by T32HL007538 (pro-

gram director: P.W. Noble), T32HL098099 (program director: J.A. Voynow), R37HL071303 (principal investigator: B.L.M. Hogan), UO1HL111018 (principal investigators: S.H. Randell, B.R. Stripp, and B.L.M. Hogan), Duke University Chair's Research Award (to C.E. Barkauskas), and the Imaging Special Shared Facility (principal investigator: D.R. Keene) of the Shriners Hospitals for Children, Portland, Oregon, USA.

Received for publication January 14, 2013, and accepted in revised form April 11, 2013.

Address correspondence to: Brigid Hogan, 388 Nanaline Duke Building, Box 3709, Duke University Medical Center, Durham, North Carolina 27710, USA. Phone: 919.684.8085; Fax: 919.684.8592; E-mail: brigid.hogan@dm.duke.edu.

Barry R. Stripp's present address is: Regenerative Medicine Institute, Cedars-Sinai Medical Center, Los Angeles, California, USA.

Paul W. Noble's present address is: Department of Medicine, Cedars-Sinai Medical Center, Los Angeles, California, USA.

1. Kumar PA, et al. Distal airway stem cells yield alveoli in vitro and during lung regeneration following H1N1 influenza infection. *Cell*. 2011;147(3):525–538.
2. Kauffman SL. Cell proliferation in the mammalian lung. *Int Rev Exp Pathol*. 1980;22:131–191.
3. Butler JP, Loring SH, Patz S, Tsuda A, Yablonskiy DA, Mentzer SJ. Evidence for adult lung growth in humans. *N Engl J Med*. 2012;367(3):244–247.
4. Wansleeben C, Barkauskas CE, Rock JR, Hogan BLM. Stem cells of the adult lung: their development and role in homeostasis, regeneration, and disease. *WIREs Dev Biol*. 2013;2:131–148.
5. Vasilescu DM, et al. Assessment of morphometry of pulmonary acini in mouse lungs by nondestructive imaging using multiscale microcomputed tomography. *Proc Natl Acad Sci U S A*. 2012; 109(42):17105–17110.
6. American Thoracic Society. Definitions, epidemiology, pathophysiology, diagnosis, and staging. *Am J Respir Crit Care Med*. 1995;152(pt 2):S78–S83.
7. Raghu G, et al. An official ATS/ERS/JRS/ALAT statement: idiopathic pulmonary fibrosis: evidence-based guidelines for diagnosis and management. *Am J Respir Crit Care Med*. 2011;183(6):788–824.
8. Tsuji T, Aoshiba K, Nagai A. Alveolar cell senescence in patients with pulmonary emphysema. *Am J Respir Crit Care Med*. 2006;174(8):886–893.
9. Aoshiba K, Nagai A. Senescence hypothesis for the pathogenetic mechanism of chronic obstructive pulmonary disease. *Proc Am Thorac Soc*. 2009; 6(7):596–601.
10. Steele MP, Schwartz DA. Molecular mechanisms in progressive idiopathic pulmonary fibrosis. *Annu Rev Med*. 2013;64:265–276.
11. Kapanci Y, Weibel ER, Kaplan HP, Robinson FR. Pathogenesis and reversibility of the pulmonary lesions of oxygen toxicity in monkeys. II. Ultrastructural and morphometric studies. *Lab Invest*. 1969;20(1):101–118.
12. Evans MJ, Cabral LJ, Stephens RJ, Freeman G. Renewal of alveolar epithelium in the rat following exposure to NO_2. *Am J Pathol*. 1973;70(2):175–198.
13. Rock JR, et al. Multiple stromal populations contribute to pulmonary fibrosis without evidence for epithelial to mesenchymal transition. *Proc Natl Acad Sci U S A*. 2011;108(52):E1475–E1483.
14. Degryse AL, Lawson WE. Progress toward improving animal models for idiopathic pulmonary fibrosis. *Am J Med Sci*. 2011;341(6):444–449.
15. Barker N, et al. Lgr5(+ve) stem cells drive self-renewal in the stomach and build long-lived gastric units in vitro. *Cell Stem Cell*. 2010;6(1):25–36.
16. Lu CP, et al. Identification of stem cell populations in sweat glands and ducts reveals roles in homeostasis and wound repair. *Cell*. 2012;150(1):136–150.
17. Mascre G, et al. Distinct contribution of stem and progenitor cells to epidermal maintenance. *Nature*. 2012;489(7415):257–262.
18. Gonzalez RF, Allen L, Gonzales L, Ballard PL, Dobbs LG. HTII-280, a biomarker specific to the apical plasma membrane of human lung alveolar type II cells. *J Histochem Cytochem*. 2010;58(10):891–901.
19. Snippert HJ, et al. Intestinal crypt homeostasis results from neutral competition between symmetrically dividing Lgr5 stem cells. *Cell*. 2010;143(1):134–144.
20. Chapman HA, et al. Integrin alpha6beta4 identifies an adult distal lung epithelial population with regenerative potential in mice. *J Clin Invest*. 2011; 121(7):2855–2862.
21. Tropea KA, et al. Bronchioalveolar stem cells increase after mesenchymal stromal cell treatment in a mouse model of bronchopulmonary dysplasia. *Am J Physiol Lung Cell Mol Physiol*. 2012;302(9):L829–L837.
22. Kim CF, et al. Identification of bronchioalveolar stem cells in normal lung and lung cancer. *Cell*. 2005;121(6):823–835.
23. Zheng D, et al. Regeneration of alveolar type I and II cells from Scgb1a1-expressing cells following severe pulmonary damage induced by bleomycin and influenza. *PloS One*. 2012;7(10):e48451.
24. Gonzalez RF, Allen L, Dobbs LG. Rat alveolar type I cells proliferate, express OCT-4, and exhibit phenotypic plasticity in vitro. *Am J Physiol Lung Cell Mol Physiol*. 2009;297(6):L1045–L1055.
25. McQualter JL, Yuen K, Williams B, Bertoncello I. Evidence of an epithelial stem/progenitor cell hierarchy in the adult mouse lung. *Proc Natl Acad Sci U S A*. 2010;107(4):1414–1419.
26. Murphy JR. Corynebacterium diphtheriae. In: Baron S, ed. *Medical Microbiology*. 4th ed. Galveston, Texas, USA: University of Texas Medical Branch at Galveston; 1996:Chapter 32.
27. Mitamura T, Higashiyama S, Taniguchi N, Klagsbrun M, Mekada E. Diphtheria toxin binds to the epidermal growth factor (EGF)-like domain of human heparin-binding EGF-like growth factor/diphtheria toxin receptor and inhibits specifically its mitogenic activity. *J Biol Chem*. 1995;270(3):1015–1019.
28. Salaun B, et al. CD208/dendritic cell-lysosomal associated membrane protein is a marker of normal and transformed type II pneumocytes. *Am J Pathol*. 2004;164(3):861–871.
29. Sisson TH, et al. Targeted injury of type II alveolar epithelial cells induces pulmonary fibrosis. *Am J Respir Crit Care Med*. 2010;181(3):254–263.
30. Hama H, et al. Scale: a chemical approach for fluorescence imaging and reconstruction of transparent mouse brain. *Nat Neurosci*. 2011;14(11):1481–1488.
31. Bostrom H, Gritli-Linde A, Betsholtz C. PDGF-A/PDGF alpha-receptor signaling is required for lung growth and the formation of alveoli but not for early lung branching morphogenesis. *Dev Dyn*. 2002;223(1):155–162.
32. Hamilton TG, Klinghoffer RA, Corrin PD, Soriano P. Evolutionary divergence of platelet-derived growth factor alpha receptor signaling mechanisms. *Mol Cell Biol*. 2003;23(11):4013–4025.
33. Chen L, Acciani T, Le Cras T, Lutzko C, Perl AK. Dynamic regulation of platelet-derived growth factor receptor α expression in alveolar fibroblasts during realveolarization. *Am J Respir Cell Mol Biol*. 2012;47(4):517–527.
34. Lo B, Hansen S, Evans K, Heath JK, Wright JR. Alveolar epithelial type II cells induce T cell tolerance to specific antigen. *J Immunol*. 2008;180(2):881–888.
35. Chen F, et al. Hop is an unusual homeobox gene that modulates cardiac development. *Cell*. 2002; 110(6):713–723.
36. Yin Z, et al. Hop functions downstream of Nkx2.1 and GATA6 to mediate HDAC-dependent negative regulation of pulmonary gene expression. *Am J Physiol Lung Cell Mol Physiol*. 2006;291(2):L191–L199.
37. Chen H, et al. Airway epithelial progenitors are region specific and show differential responses to bleomycin-induced lung injury. *Stem Cells*. 2012; 30(9):1948–1960.
38. Lee JH, et al. SPC H2B-GFP mice reveal heterogeneity of surfactant protein C-expressing lung cells. *Am J Respir Cell Mol Biol*. 2013;48(3):288–298.
39. Teisanu RM, et al. Functional analysis of two distinct bronchiolar progenitors during lung injury and repair. *Am J Respir Cell Mol Biol*. 2011;44(6):794–803.
40. McGowan SE, Torday JS. The pulmonary lipofibroblast (lipid interstitial cell) and its contributions to alveolar development. *Annu Rev Physiol*. 1997; 59:43–62.
41. Kaplan NB, Grant MM, Brody JS. The lipid interstitial cell of the pulmonary alveolus. Age and species differences. *Am Rev Respir Dis*. 1985;132(6):1307–1312.
42. Bastacky J, Goerke J. Pores of Kohn are filled in normal lungs: low-temperature scanning electron microscopy. *J Appl Physiol*. 1992;73(1):88–95.
43. Namati E, Thiesse J, de Ryk J, McLennan G. Alveolar dynamics during respiration: are the pores of Kohn a pathway to recruitment? *Am J Respir Cell Mol Biol*. 2008;38(5):572–578.
44. Lopez-Garcia C, Klein AM, Simons BD, Winton DJ. Intestinal stem cell replacement follows a pattern of neutral drift. *Science*. 2010;330(6005):822–825.
45. Qunn L, et al. Hyperplastic epithelial foci in honeycomb lesions in idiopathic pulmonary fibrosis. *Virchows Arch*. 2002;441(3):271–278.
46. Huszar G, Maiocco J, Naftolin F. Monitoring of collagen and collagen fragments in chromatography of protein mixtures. *Anal Biochem*. 1980;105(2):424–429.
47. Savov J, Silbajoris R, Young SL. Mechanical ventilation of rat lung: effect on surfactant forms. *Am J Physiol*. 1999;277(2 pt 1):L320–L326.
48. Rock JR, et al. Basal cells as stem cells of the mouse trachea and human airway epithelium. *Proc Natl Acad Sci U S A*. 2009;106(31):12771–12775.
49. Randell SH, Fulcher ML, O'Neal W, Olsen JC. Primary epithelial cell models for cystic fibrosis research. *Methods Mol Biol*. 2011;742:285–310.